Valery Andrushchenko
Zoya Leonenko
David Cramb
Hans van de Sande
Hal Wieser
Department of Chemistry, University of Calgary, 2500 University Drive, NW, Calgary, Alberta, Canada, T2N 1N4

Received 5 November 2001; accepted 8 January 2002

Vibrational CD (VCD) and Atomic Force Microscopy (AFM) Study of DNA Interaction with Cr^{3+} Ions: VCD and AFM Evidence of DNA Condensation

Abstract: *The interaction of natural calf thymus DNA with Cr^{3+} ions was studied at room temperature by means of vibrational CD (VCD) and infrared absorption (ir) spectroscopy, and atomic force microscopy (AFM). Cr^{3+} ion binding mainly to N_7 (G) and to phosphate groups was demonstrated. ψ-Type VCD spectra resembling electronic CD (ECD) spectra, which appear during ψ-type DNA condensation, were observed. These spectra are characterized mainly by an anomalous, severalfold increase of VCD intensity. Such anomalous VCD spectra were assigned to DNA condensation with formation of large and dense particles of a size comparable to the wavelength of the probing ir beam and possessing large-scale helicity. Atomic force microscopy confirmed DNA condensation by Cr^{3+} ions and the formation of tight DNA particles responsible for the ψ-type VCD spectra. Upon increasing the Cr^{3+} ion concentration the shape of the condensates changed from loose flower-like structures to highly packed dense spheres. No DNA denaturation was seen even at the highest concentration of Cr^{3+} ions studied. The secondary structure of DNA remained in a B-form before and after the condensation. VCD and ir as well as AFM proved to be an effective combination for investigating DNA condensation. In addition to the ability of VCD to determine DNA condensation, VCD and ir can in the same experiment provide unambiguous information about the secondary structure of DNA contained in the condensed particles.* © 2002 Wiley Periodicals, Inc. Biopolymers 61: 243–260, 2002

Keywords: *DNA condensation; metal ions; CD; vibrational CD spectroscopy; infrared spectroscopy; atomic force microscopy*

INTRODUCTION

DNA condensation is a process of great interest, which plays an important role in DNA packing in a living cell. DNA condensation is also a very important step in the process of gene delivery for gene therapy.

The length of DNA may exceed 10^5 times the length of the cell.[1] At the same time, DNA must fit into a very small space inside a cell nucleus, occupy-

Correspondence to: Hal Wieser; email: hwieser@ucalgary.ca
Contract grant sponsor: Natural Sciences and Research Council of Canada, IIPP, and Travis Chemicals

ing 10^4–10^6 times less volume than it does when free in solution.[2] In order to achieve such a high level of compaction, a DNA molecule transforms (or several molecules assemble) into higher ordered three-dimensional structures. This process is called DNA condensation.[3]

DNA condensation can be induced by the addition of various condensing agents or combinations thereof. These can be naturally occurring polyamines (spermine and spermidine), cobalt hexamine,[3–6] trivalent (or higher valence) metal ions,[3,7–10] protamine,[11] polylysine,[12] neutral polymers (e.g., polyethylene oxide) along with high concentrations of monovalent salt (e.g., NaCl) (the latter one produces so-called ψ-DNA, where ψ is the acronym for *P*olymer-and-*S*alt-*I*nduced)[13] and even positively charged surfaces,[14] and cationic phospholipid bilayers.[15]

Based on calculations with the counterion condensation theory developed by Manning,[16] condensation of a polymer can become thermodynamically favorable when solvent–DNA interactions become less favorable than DNA–DNA interactions. This condition is achieved when a sufficient degree of negative DNA phosphate charges is neutralized.[17] Wilson and Bloomfield have calculated this degree of neutralization to be 89–90%.[17] According to Manning's theory,[16] only trivalent (or higher valence) ions are able to induce this degree of phosphate charge neutralization in aqueous solutions at room temperature. However, the DNA condensation process cannot be described only by electrostatic effects employed in the counterion condensation theory.[4] Site-specific interactions of metal ions with DNA and formation of condensing agent-mediated cross-links between different parts of the DNA molecule (molecules) may also be important in the DNA condensation process.[8,10,18–21]

DNA condensation has been studied by different techniques, including ultraviolet (uv) and electronic CD (ECD) spectroscopy,[8,22–27] light scattering,[2,17,19,28,29] ir spectroscopy,[9,10] fluorescence microscopy,[30] electron microscopy,[2,19,31,32] and recently atomic force microscopy (AFM).[1,12,33–35]

One of the most pronounced spectroscopic manifestations of DNA condensation, first noticed for ψ-type condensation, is an enormously large ECD spectrum. CD intensity increases up to several orders of magnitude compared to normal ECD of B-DNA.[22–25,36] Later it was found that ψ-type ECD spectra can be obtained not only in polymer-and-salt induced DNA condensation but also with other condensing agents (including trivalent metal ions) and at different DNA concentrations.[8,25] ψ-Type ECD spectra can be obtained for DNA with molecular weight ranging from 1.5×10^5 to 3.3×10^6 Da (~230 to ~5000 base pairs, respectively).[24] The anomalous ECD signals are observed not only in proper experimental conditions in vitro, but also in the condensed chromatin of various systems in vivo.[37]

The rather sharp melting transition of the ψ-form (within 5–10°C) strongly suggests an ordered structure of condensed particles.[23] Size and shape of the particles varies depending on the experimental conditions (e.g., concentration of DNA and condensing agent). In very dilute aqueous solutions (~1 μg/mL), DNA usually condenses with formation of toroids and rods with very similar morphology and size.[3,4] At higher DNA concentrations irregular globular structures, flower-like structures and amorphous shapes are formed.[1,12,37,38] The particle size varies from 80–100 nm to 30 μm or more, depending on the conditions.[3,4,39]

In addition to the anomalous intensity, ψ-type ECD spectra possess other characteristic features, such as long "tails" in nonabsorbing regions due to light scattered by condensed particles.[23,26,40] While the shape of the spectra is relatively reproducible for the same system, the magnitude varies from preparation to preparation,[40] indicating that the ψ-type spectra are dependent on the supramolecular structure of the condensed particles rather than on any intrinsic property of the constituent materials.[37]

Different theoretical approaches have been proposed attempting to explain the anomalous ECD spectra.[23,26,40,41] The most complete theory[37,42,43] explains light interaction with large aggregates and anomalously large CD spectra by long-range coupling of chromophores. In order for such a long-range coupling to take place, three criteria should be satisfied: (a) the size of a particle should be at least one-quarter the wavelength at the absorption maximum; (b) particle density should be higher than a certain limiting value; and (c) a particle should have more or less three-dimensional packing arrangement.[42] An additional, forth criterion should be satisfied in order to induce anomalously large CD spectra, i.e., a particle should have a large-scale chiral structure, which could interact differently with right and left circularly polarized light. When the dimensions of a chiral object are similar to the wavelength of the incident light, the large-scale handedness of the object will have a much greater effect in enhancing or suppressing the absorption of circularly polarized light than when the chiral object is small compared to the wavelength.[37]

X-ray and Raman data suggest that the secondary structure of condensed DNA resembles most closely the B-conformation.[44,45] It is important to note that it is the tertiary helical ordering of the DNA molecules

that produces the large CD values. Any random packing of nucleic acids will not cause any changes in CD except those resulting from changes in secondary structure, which are significantly smaller in amplitude.[26] Furthermore, any changes in ECD that might occur as a result of changes in the secondary structure of DNA in the condensed state will be obscured by much stronger ECD arising from a suprahelical structure.[40] This makes it difficult to monitor the DNA secondary structure inside the condensed particles by ECD and uv. In order to obtain this information, additional techniques like x-ray or Raman spectroscopy are required.[44,45] Since different techniques usually need different experimental conditions, the condensation process can be significantly altered in the different measurements.[37,40]

The present work uses VCD and AFM to study DNA condensation induced by Cr^{3+} ions. VCD is a relatively new technique, which was used successfully in various investigations of nucleic acids.[46–56] While possessing the advantages of ECD, VCD provides all the benefits of ir over conventional uv. For example, ir can be used to determine unambiguously nucleic acid conformations.[57–59] One of the aims of the present study was to determine whether VCD can detect DNA condensation analogously to ECD by the appearance of anomalous VCD spectra. If successful, VCD could emerge as a tool able to monitor DNA condensation while determining simultaneously the secondary structure, thereby resolving the problem of different experimental conditions.

AFM is a complementary technique, which has an advantage over electron microscopy for observing DNA in the liquid phase under near-physiological conditions with three-dimensional resolution. AFM was used in the present study in order to confirm the formation of condensed DNA particles, visualize the condensation process, and determine the morphologies of the particles formed.

MATERIALS AND METHODS

Sodium cacodylate and $CrCl_3 \times 6H_2O$ salts and D_2O (99.9%) were purchased from Sigma Chemicals. Sodium salt of ultrapure calf thymus DNA was obtained from Prof. D. Lando, Institute of Bio-organic Chemistry, Belarus National Academy of Sciences, Belarus (protein content $< 0.08\%$, RNA content $< 0.1\%$, ratio $A_{260}/A_{280} = 1.84$ and average molecular weight 2.5×10^7 Da) and used without further purification.[60] Double-distilled water was used in all experiments.

All solutions were prepared in $10^{-2}M$ cacodylic buffer with the pH adjusted to 6.5 ± 0.5. DNA was fragmentized by ultrasonication to reduce its size to an average length of 850 base pairs (molecular weight 5.6×10^5 Da) as determined by gel electrophoresis. Initial stock solutions of DNA and metal ions were prepared in aqueous cacodylic buffer. Complete deuterium exchange was achieved by lyophilizing and redissolving all solutions three times in D_2O. The concentration of the DNA stock solutions after final dissolution in D_2O was determined from uv absorption at 260 nm.

DNA samples for spectroscopy were contained in a demountable cell (International Crystal Laboratories, Inc.) composed of two BaF_2 windows separated by a 50 μm Teflon spacer. The DNA stock solution (30 μL) was deposited directly on the bottom cell window. Metal ion solution (15 μL) of appropriate concentration was added to the DNA dropwise with continuous stirring and then covered with the top window. The final concentration of DNA in the cell was 30 mg/mL, or 0.1*M* DNA phosphate ([P]). Cr^{3+} concentration was varied from 0 to 0.3*M*, or 0 to 3 [Cr]/[P] (ratio of the molar concentrations of metal ion and DNA phosphates). The temperature was 23 ± 1°C controlled with a copper-constantan thermocouple (Omega Technology Company, Inc.).

All VCD and absorption spectra were measured in the range of 1800–750 cm^{-1} in D_2O with the VCD spectrometer described elsewhere.[61] For the VCD spectra, 7500 ac scans were accumulated (1 h, 40 min) and ratioed against 500 dc scans all at 8 cm^{-1} resolution. For the absorption spectra, 500 dc scans were collected at the same resolution. The VCD spectra were corrected for polarization artifacts by subtracting the spectra of the solvent obtained at the same conditions. Absorption and VCD spectra were interpolated with a 4-point cubic spline algorithm (interpolation factor 8) supplied with the Lab Calc package (Lab Calc, 1992). The wavenumber interval between 1150 and 1450 cm^{-1} was cut out from the plots of the spectra. This interval contains a strong absorption arising from deformation mode of D_2O and overlapping all DNA features.

The relative or normalized intensity of the absorption peaks or VCD couplets in arbitrary units (R or N, respectively) vs Cr^{3+} concentration were plotted as

$$R = I_i/I_0,$$

$$N = (I_i - I_{min})/(I_{max} - I_{min}),$$

where I_i is the intensity of an absorption peak or VCD couplet for nucleic acid at the *i*th metal ion concentration, I_0 is the same without metal ions, I_{min} is the minimum intensity of an absorption peak or VCD couplet encountered in the whole metal ion concentration range, and I_{max} is the corresponding maximum intensity. The metal ion concentration in the plots is shown in molar concentration (bottom axis) and as the [Cr]/[P] ratio (top axis).

AFM is a surface imaging technique with lateral resolution in units of nm and normal resolution in Å. It measures the forces acting between a probe and a sample. The instrument was operated in the magnetic A/C mode (MAC), where the magnetically coated probe oscillates near its

resonant frequency driven by an alternating magnetic field. In this mode, changes in height and phase shift are measured during the scan.[62,63] This technique has proven to be advantageous for measuring soft samples in liquid media. All images were taken using a Pico SPM microscope with an AFMS-165 scanner (Molecular Imaging Inc., Phoenix, AZ). Au–Cr coated Maclevers were used for MAC mode imaging (Molecular Imaging Inc., Phoenix, AZ, 85 μm length, 0.5–0.7 N/m force constant, 20–40 kHz resonant frequency in the liquid phase). The standard MAC mode fluid cell (Molecular Imaging) was used throughout. The scanning speed was 2–3 lines/s/. Samples for AFM imaging were prepared by applying DNA solutions (850 and 3000 base pairs) with or without Cr^{3+} on modified or unmodified scratch-free ruby mica, freshly cleaved, ASTMV-2 quality (Asheville-Schoonmaker Mica Co., VA). The calf thymus DNA with 850 base pairs, fragmentized by ultrasonication, was the same as for the VCD experiments. The linearized DNA with 3000 base pairs from *Escherichia coli* was obtained from Dr. S. P. Lees-Miller, Department of Biochemistry, University of Calgary. DNA concentration was 80 μg/mL or 2.5 $\times 10^{-4}M$ in phosphate buffer. Tris EDTA (TE) buffer (25 m*M* Tris HCl, 0.5 m*M* EDTA, and 50 m*M* NaCl, pH 7.6) and distilled ultrapure (Nanopure) water were used for sample preparation. DNA molecules were adsorbed onto pure mica by adding $MgCl_2$ to the solution, or mica modified by poly-L-lysine (PLL) or 3-aminoethyl-3-ethoxosilane (APTES). To adsorb complexes, mica modified by PLL was used. After a controlled time period, the mica was gently rinsed with ultrapure water. The excess of DNA was rinsed away and the surface was imaged under water in the liquid cell.

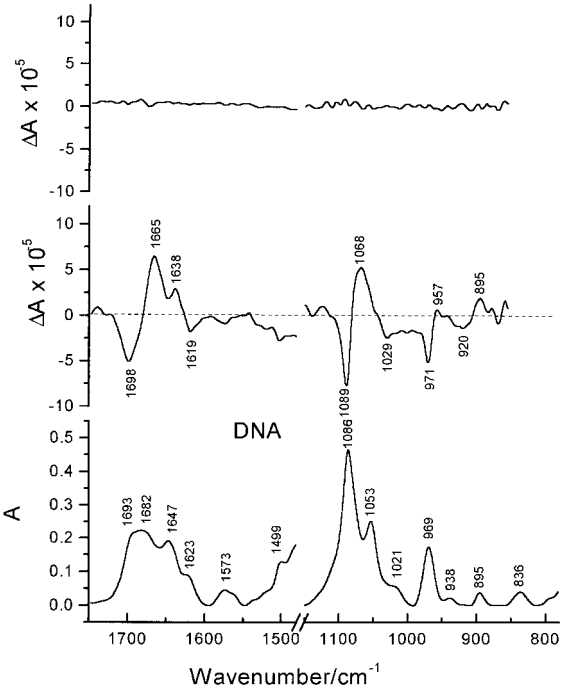

FIGURE 1 Absorption (bottom) and VCD (center) spectra of calf thymus DNA, and noise estimate for VCD spectrum (top).

RESULTS AND DISCUSSION

VCD Spectroscopy

VCD Spectrum of Calf Thymus DNA. The ir and VCD spectra of calf thymus DNA (Figure 1) are both characteristic for the B-conformation.[57–59,64–66] The assignments for the absorptions (Table I) appear to be well established for DNA. Since there is less detailed information about the VCD spectra of DNA, the most prominent VCD features are discussed below.

The absorption at 1693 cm^{-1} appearing as a shoulder (Figure 1) has been assigned to $C_2{=}O$ stretching of thymine (T), and the absorption at 1682 cm^{-1} mostly to $C_6{=}O$ stretching of guanine (G) coupled with $C_4{=}O$(T) and $C_2{=}O$ stretching of cytosine (C). The corresponding strong VCD feature at 1698(−)/1665(+) cm^{-1} can be interpreted as a superposition of several couplets arising from all these C=O vibrations possibly explaining the appearance of the slight negative shoulder at ~1689 cm^{-1}. The intensity of the positive VCD peak at 1665 cm^{-1} is significantly higher than that of the positive peak at 1638 cm^{-1}. In poly(dA) · poly(dT) and poly(dA-dT) · poly(dA-dT) both these features have about the same intensities,[66] supporting a superposition of couplets for DNA arising from carbonyl stretching modes of G, T, and C. Although it was noted that intensity of the positive $C_4{=}O$(T) VCD peak is increased compared to one at lower wavenumber for the A-form of poly(dA-dT) · poly(dA-dT),[66] it cannot be assumed that the DNA existed in the A-form, because the absorption markers at 898, 865, and 810 cm^{-1} were absent while the absorption markers for the B-form at 938, 894 and 836 cm^{-1} were clearly evident.[59,64] A weak negative couplet arising from $C_2{=}O$(T) also contributes to the 1698(−)/1665(+) cm^{-1} feature.[65,66]

The absorption band at 1647 cm^{-1} has been assigned to overlapping absorptions mostly from $C_2{=}O$(C) coupled with $C_4{=}O$(T) and $C_6{=}O$(G). The 1623 cm^{-1} absorption band likely consists of contributions from ring modes mostly of adenine (A) and also of T and C.[57] The ring mode of A gives a distinct positive VCD couplet at 1635(−)/1625(+) cm^{-1} in poly(rA) · poly(rU).[49,51] The VCD spectra of poly(dA) · poly(dT) and poly(dA-dT) · poly(dA-dT) show ring modes of A and T as a combined negative couplet at 1640(+)/1625(−) cm^{-1}.[67] The ring mode of T in d(CGCGTGCG) · d(CGCGTGCG) appears as a distinctive negative couplet at 1645(+)/1633(−)

Table I Infrared Absorption and VCD Bands of Calf Thymus DNA and Calf Thymus DNA with 0.3*M* Cr^{3+} (3 [Cr]/[P])

DNA		DNA with 3 [Cr]/[P]		
Absorption (cm^{-1})	VCD (cm^{-1})	Absorption (cm^{-1})	VCD (cm^{-1})	Assignments[46,57–59,64–66,80]
1693	1698(−)	1691	1702(−)	C_2 = O (T)
1682	1698(−)/1665(+)	1667	1689(−)/1663(+)	Mostly C_6 = O (G), coupled with C_2 = O (C) and C_4 = O (T)
1647	1638(+) ?	1647	1637(+) ?	Mostly C_2 = O (C); C_4 = O (T), coupled with C_6 = O(G)
1623	1619(−)	1619	—	Mostly ring modes of A
1573	—	1573	1565(+) ?	C = N ring (G,A)
1499	—	1500	1492(+) ?	C = N ring (C)
1086	1089(−)/1068(+)	1085	1090(−)/1069(+)	PO_2^- symmetric
1053	1060(+)	1053	1056(−)/1040(+)	C—O sugar
1021	1029(−) ?	1017	1013(+) ?	Deoxyribose ring
969	971(−)/957(+)	970	976(−)/963(+)	C—C sugar stretches
938	—	940	929(+) ?	Sugar
895	920(−)/895(+) ?	896	893(+)/878(−) ?	Sugar, B-form marker
836	—	836	—	Sugar, B-form marker

cm^{-1}.[68] The positive VCD peak at 1638 cm^{-1} in DNA (Figure 1) can therefore be ascribed to a combination of the negative couplet due to a ring mode of T at higher wavenumber, and a positive couplet due to the ring mode of A at a lower wavenumber.

The broad absorption at 1573 cm^{-1} has been assigned to a superposition of several bands arising from ring vibrations of G and A involving mainly the C═N bonds, while the 1499 cm^{-1} absorption has been assigned to a mode of C that also contains C═N stretching. Neither of these two absorptions have clearly corresponding VCD features, although the latter in particular gives rise to a distinctive couplet in oligomers with high GC content that appears consistently near 1502(+)/1498(−) cm^{-1} in the B-form and reverses signs in the Z-form.[54,55,68]

In the sugar–phosphate region the prominent absorption at 1086 cm^{-1} with its corresponding strong positive VCD couplet at 1089(−)/1068(+) cm^{-1} has been assigned to symmetric P—O stretching of the phosphate groups.[57–59] The absorption at 1053 cm^{-1} is due to a C—O sugar ring vibration. The low wavenumber component of the broad positive VCD lobe between 1070 and 1060 cm^{-1} may arise partly from this mode.[69] The absorption at 1021 cm^{-1} has also been assigned to deoxyribose ring vibrations. The negative VCD peak at 1029 cm^{-1} may possibly be ascribed to this mode.[69] The 969 cm^{-1} absorption assigned to C—C sugar stretching vibrations yields either the negative VCD peak at 971 cm^{-1}, or the positive couplet at 971(−)/957(+) cm^{-1}. C—O sugar vibrations have been assigned to the absorptions at 938, 895, and 836 cm^{-1}.

Cr^{3+} Binding to DNA. The absorption and VCD spectra of DNA with Cr^{3+} ions at 0.6 and 3 [Cr]/[P] are shown in Figures 2 and 3, respectively. The absorption and VCD spectra for several key concentrations of Cr^{3+} are displayed in Figures 4 and 5, respectively. The changes in position and intensity of absorption band and changes of the corresponding VCD couplet are plotted in Figure 6 for the carbonyl mode and in Figure 7 for the symmetric phosphate vibration. To emphasize the differences of the changes in absorption and VCD, the intensity changes from Figure 6 are presented on one scale without normalization in Figure 8.

Upon adding Cr^{3+} ions to DNA up to 0.036*M* Cr^{3+} (0.36 [Cr]/[P], spectra not shown), the absorption and VCD spectra undergo some changes in intensity (■ and △, respectively, in Figure 6) and peak position (● in Figure 6, absorption only). The main intensity changes of the VCD couplets largely follow those of the corresponding absorptions in this range of metal ion concentration. Further increasing Cr^{3+} concentration affects the VCD spectra extensively, while changes in the absorption spectra, manifested mostly

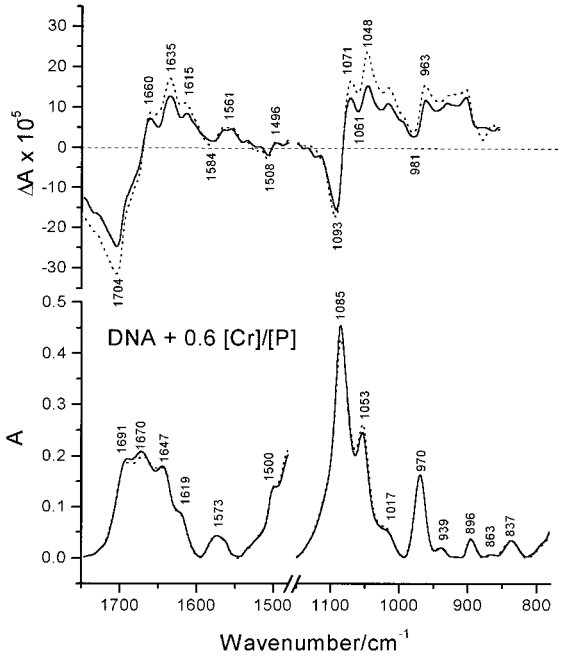

FIGURE 2 Absorption (bottom) and VCD (top) spectra of DNA + 0.06*M* Cr^{3+} (0.6 [Cr]/[P]). The solid and doted lines correspond to the spectra taken 1 h 40 min and 3 h 20 min, respectively, after preparing the sample.

in peak position and intensities, are not so pronounced. The peak position of the main carbonyl absorption shifts from 1682 to ~1672 cm^{-1} and further to 1667 cm^{-1} as Cr^{3+} concentration reaches 0.36 and 3 [Cr]/[P], respectively (Figures 4 and 6). The peak intensities of the carbonyl and the symmetric phosphate absorptions decrease up to ~0.1 [Cr]/[P] at first and then sharply increase with increasing Cr^{3+} concentration up to 0.25 [Cr]/[P] (Figures 6 and 7). The decrease of the absorption bands at low Cr^{3+} concentrations can be ascribed to metal ions binding mainly to phosphate groups. This will effectively neutralize the negative charge on the phosphates and stabilize the double-helical structure as reflected in increased hypochromicity for ir absorptions in the base region compared to low salt conditions.[9,70] However, the downward shift of the 1682 cm^{-1} absorption signals direct metal binding to the bases to some extent.[9,10,70] The significant sharp intensity increase of the base and phosphate absorptions upon increasing Cr^{3+} concentration from 0.12 to 0.25 [Cr]/[P] indicates direct metal binding to the phosphate groups and the bases.[10] Changes of the 1682 cm^{-1} absorption might be connected with Cr^{3+} binding to carbonyl groups of G, C, and T since they all contribute to this vibration. However, significant direct metal binding to carbonyl groups involved in Watson–Crick hydrogen bonding may be excluded because it should be accompanied by hydrogen-bond disruption.[70] No evidences of DNA denaturation to any extent even at the highest Cr^{3+} concentration can be found in either absorption or the VCD (Figures 2 and 3). Moreover, the main changes in the 1700–1600 cm^{-1} range were connected with metal binding to N_7(G).[9,10,70–72] Experimental results and ab initio calculations show that direct metal ion binding to N_7 (G) may reenforce Watson–Crick hydrogen bonding by charge redistribution, thus inducing the main changes in this region.[72,73] In addition, examination of other absorptions of C and T residues rules out direct Cr^{3+} binding to these bases. Metal ion binding to C gives an absorption band around 1550 cm^{-1},[74,75] which is absent in our spectra (Figures 2 and 3). Cr^{3+} binding to C═O_2(T) can also be excluded because no significant wavenumber shift of the 1693 cm^{-1} absorption is observed up to 3 [Cr]/[P]. Therefore, all spectral changes at Cr^{3+} concentration up to 0.25 [Cr]/[P] are most likely induced by direct metal ion binding to N_7(G) and to phosphate groups. This conclusion is further supported by the fact that Cr^{3+} ions have been shown to bind preferably to GC-rich DNA.[76,77] However, indirect Cr^{3+} binding to AT base pairs via water molecules cannot be excluded.[10] Noteworthy is the sharp increase of the 1682 cm^{-1} absorption within a relatively narrow metal ion concentration range, which suggests a high cooperativity of the binding process. Similar highly cooperative processes of di-

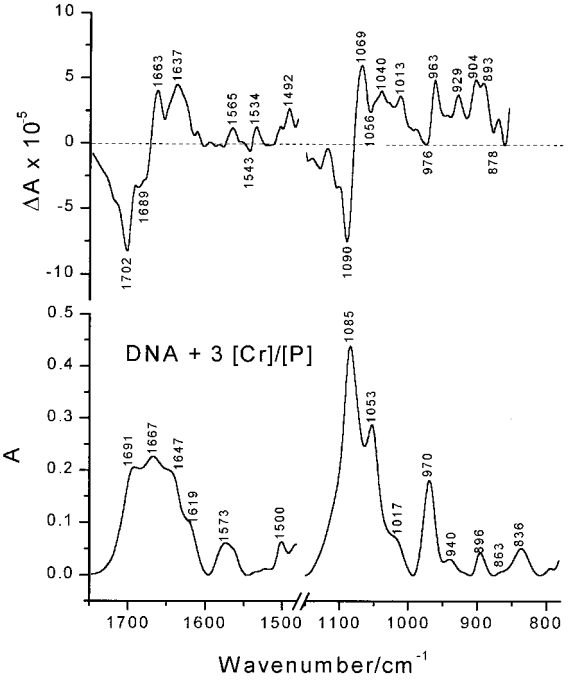

FIGURE 3 Absorption (bottom) and VCD (top) spectra of DNA + 0.3*M* Cr^{3+} (3 [Cr]/[P]).

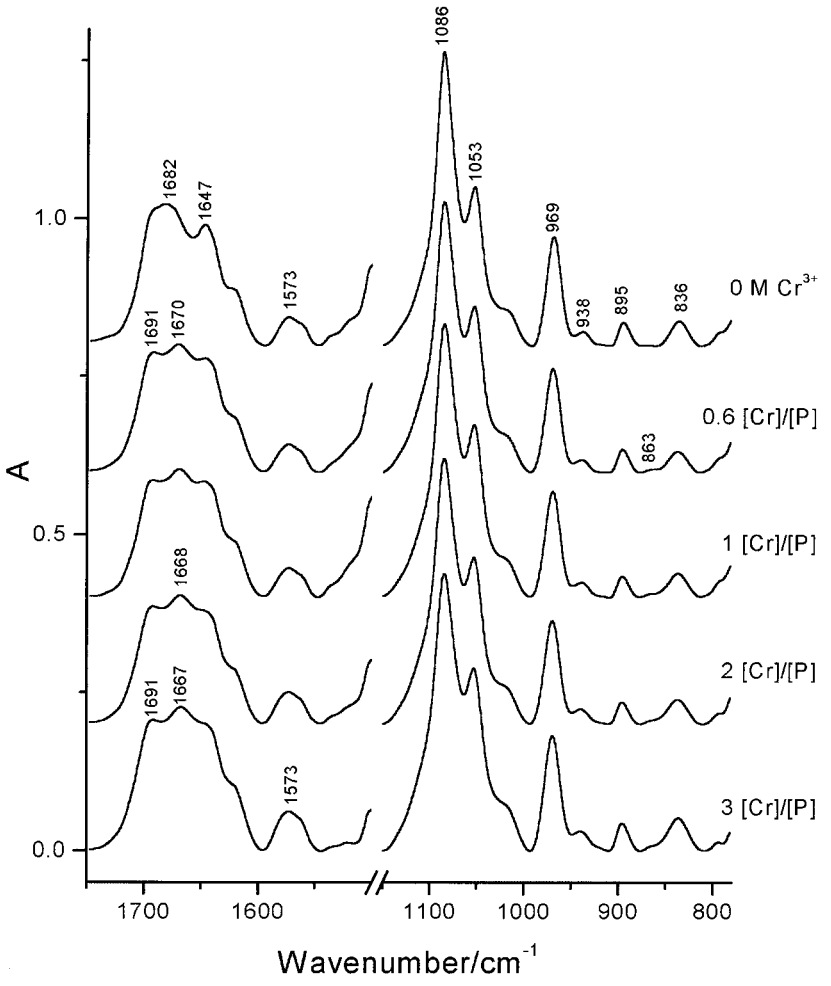

FIGURE 4 Absorption spectra of DNA and DNA with Cr^{3+} ions at different [Cr]/[P] ratios. All spectra are plotted in the same scale.

valent metal ion binding to DNA have been described before.[9,70,78,79]

Cr^{3+}-Induced DNA Condensation. Raising the Cr^{3+} ion concentration above 0.36 [Cr]/[P] sharply decreases absorption intensities in the nitrogen base and sugar–phosphate regions (Figures 6 and 7). This intensity decrease is accompanied by a further shift of the carbonyl absorption (Figure 6), indicating continuing Cr^{3+} binding to N_7 (G). However, the most dramatic changes happen in VCD (Figures 2 and 5). The anomalous almost fourfold increase in amplitude occurs for the main VCD couplets in both the nitrogen base and sugar–phosphate regions, whereas the corresponding absorption intensities decrease by about 30% (Figures 4, 5, and 8). The shape of the VCD couplets also changes, most prominently displayed by the apparent significant increase of the positive VCD peaks at 1635 and 1048 cm^{-1} (Figures 2 and 5). These two peaks, being much less intense compared to the 1665 and 1068 cm^{-1} counterparts in the VCD spectrum of DNA without Cr^{3+} ions (Figure 1), became at 0.6 [Cr]/[P] considerably more intense than those at 1665 and 1068 cm^{-1}. It should be noted that all these changes, namely in the amplitude of the VCD couplets as well as in the intensity redistribution between the positive VCD peaks at 1660 vs. 1635 cm^{-1} as well as 1071 vs 1048 cm^{-1}, became more pronounced after repeating the measurements in about 1 hour and 40 minutes (Figure 2). Repeating the measurements at a later time did not show significant spectral changes any further (spectra not shown).

Within the context of the existing theory,[37,42,43] the enormously increased amplitudes of VCD couplets observed at experimental conditions favoring DNA condensation can be attributed to ψ-type VCD spectra. In addition, "tails" are seen in the VCD spectra at wavenumbers higher than 1700 cm^{-1} (Figure 5), i.e.,

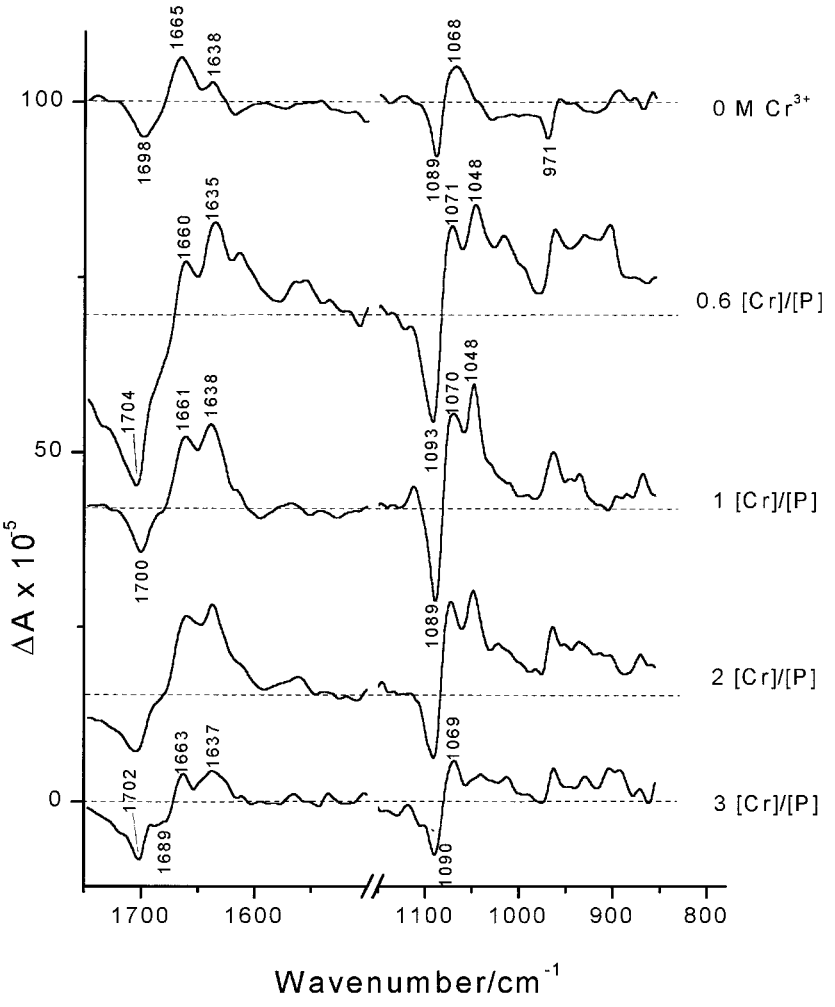

FIGURE 5 VCD spectra of DNA and DNA with Cr^{3+} ions at different [Cr]/[P] ratios. All spectra are plotted in the same scale.

in a region where no absorption occurs. According to the theory, ψ-type CD spectra can be produced within the spectral region of an absorption band when the size of a particle (molecular aggregate) is comparable to the wavelength of the incident light. The particle must be three-dimensional with sufficiently high density and a large-scale chirality. Therefore, the VCD spectra suggest that the condensates of DNA produced by Cr^{3+} ions in the experimental conditions employed in the present study are chiral particles with regular arrangements of DNA double helices within them. The particles are relatively dense and large. The size of the particles is of the order of $\sim$2–10 μm estimated from the range of wavelengths of the absorptions where the anomalous VCD occurs.

It was shown that DNA condensation reduces the intensity of the ir bands of DNA in the regions of nitrogen base and phosphate absorptions.[9,10] A similar sharp intensity decrease of the carbonyl and symmetric phosphate absorption bands can be seen in Figures 6 and 7. This represents an additional confirmation of the DNA condensation that occurs at Cr^{3+} concentrations higher than 0.6 [Cr]/[P] in the present study. Cr^{3+}-induced DNA condensation examined by electron microscopy indicated that the condensation process occurs for [Cr]/[P] ratio between 0.5 and 3.[7] A similar [Cr]/[P] concentration range for DNA condensation was obtained in a recent Fourier transform infrared (FTIR) investigation.[10] Since the DNA concentration, molecular weight, and other experimental conditions in both studies were different from the present work, some differences may exist in the [Cr]/[P] ratio at which DNA condensation occurred in the three studies.

Increasing Cr^{3+} concentration to 1 [Cr]/[P] and further to 2 [Cr]/[P] produces similarly shaped VCD spectra as in the case of 0.6 [Cr]/[P] (Figure 5). However, the amplitude of both main VCD couplets

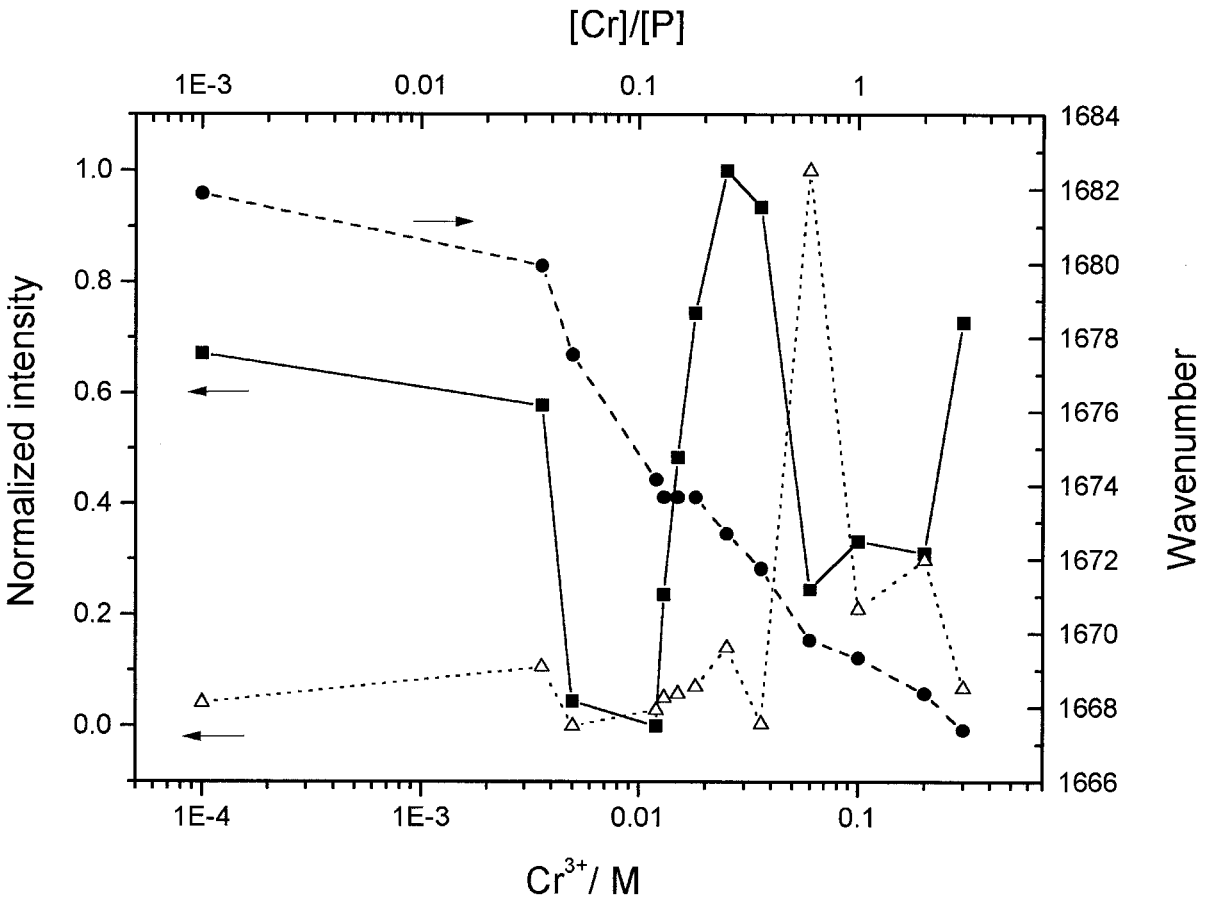

FIGURE 6 Normalized absorption and VCD intensity (left axes) and absorption peak position (right axes) vs Cr^{3+} concentration for the carbonyl 1682 cm^{-1} absorption: (■) intensity of absorption peak; (●) absorption peak position; (△) amplitude of VCD couplet.

is significantly lower and only slightly increased (about 1.5 fold) compared to the DNA without metal ions (Figures 5–7). The intensity of the positive VCD peaks at 1638 and 1048 cm^{-1} approaches that of the 1661 and 1070 cm^{-1} peaks, respectively. Repeating of the measurements with 1 [Cr]/[P] and 2 [Cr]/[P] (spectra not shown) in about 1 hour and 40 minutes produces slightly increased intensity and changes in shape of the VCD couplets similar to those obtained at 0.6 [Cr]/[P]. The changes of the spectra with time toward those characteristic for ψ-type VCD spectra at 0.6, 1, and 2 [Cr]/[P] show relatively slow kinetics of the DNA condensation (within 30 min to several hours), which is in agreement with the data of other authors.[3] Further increasing Cr^{3+} concentration up to 3 [Cr]/[P] returns the intensity of both main VCD couplets to the values obtained for DNA without Cr^{3+} ions (Figures 3 and 5–7). However, the shape of the VCD features, particularly in the base region, is noticeably altered compared to the shape of the VCD signal of DNA without metal ions. The negative shoulder at 1689 cm^{-1} becomes more pronounced. The positive lobe of the carbonyl couplet appears at 1663 cm^{-1}. The positive peak at 1637 cm^{-1} is still quite intense and comparable to the one at 1663 cm^{-1}, similar to its appearance at 1 and 2 [Cr]/[P]. In contrast to those spectra, the 1048 cm^{-1} positive peak in the phosphate region completely disappears at 3 [Cr]/[P]. The downshift of the positive part of the carbonyl couplet to 1663 cm^{-1} is reminiscent of the downward shift of the corresponding carbonyl absorption band to 1667 cm^{-1} (Figure 3). Due to the shift of this carbonyl band, the absorption shoulder at 1691 cm^{-1} assigned to $C_2{=}O$ mode of T becomes clearly visible as a separate peak. Concurrent with these changes, the shift of the VCD couplet corresponding to the 1667 cm^{-1} absorption to 1689(−)/1663(+) cm^{-1} clearly separates this couplet from the contribution of the negative VCD peak at 1702 cm^{-1}. A large number of fairly strong VCD features can be noted in the sugar–phosphate region (Figure 3). This multitude of VCD features compared to the spectrum of DNA without

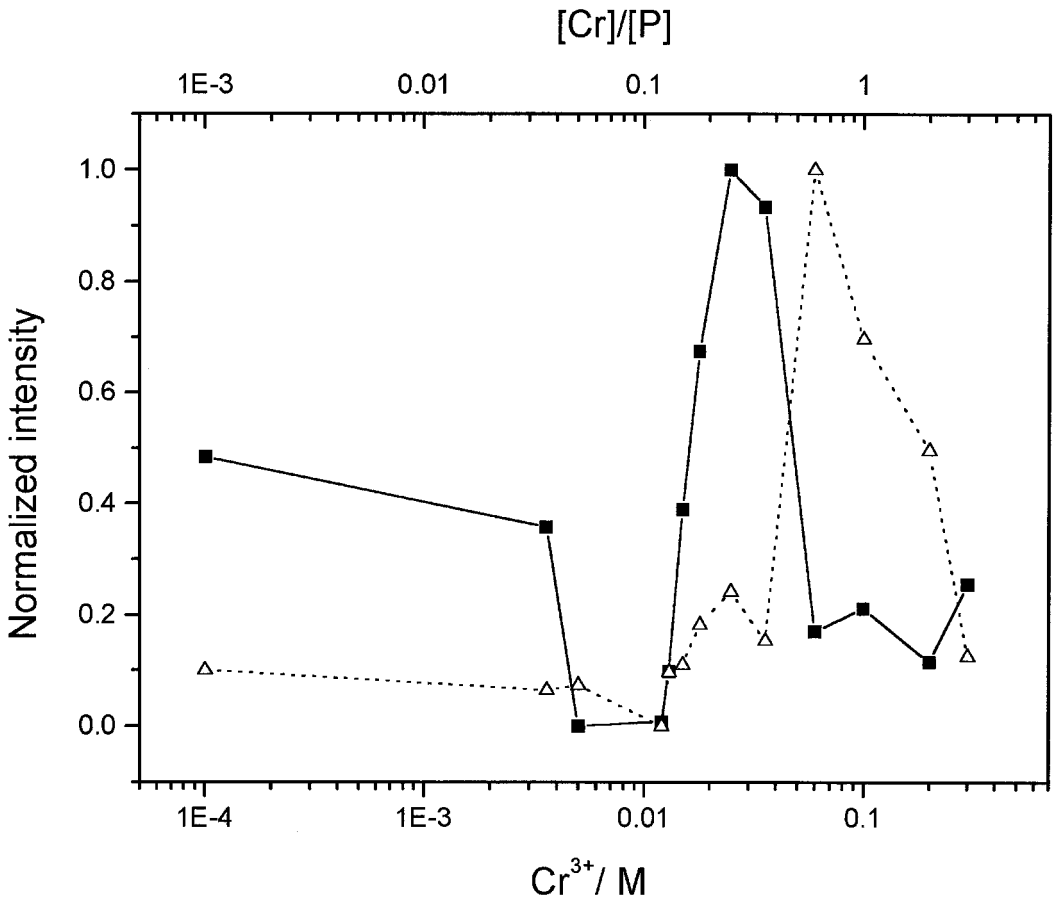

FIGURE 7 Normalized absorption and VCD intensity vs Cr^{3+} concentration for the symmetric phosphate absorption band at 1086 cm^{-1}: (■) intensity of absorption peak; (△) amplitude of VCD couplet.

metal ions might be attributed to a greater variety of the phosphate orientations fixed by bound Cr^{3+} ions.

Comparison of the VCD spectra at different Cr^{3+} concentrations in Figure 5 shows that ψ-type VCD spectra possess another characteristic feature in addition to the increased amplitude of the main VCD couplets—namely the relative intensity redistribution between the positive peaks at 1660 and 1635 cm^{-1} in the base region, and between the positive peaks at 1071 and 1048 cm^{-1} in the sugar–phosphate region. During this redistribution the intensity of the 1635 and 1048 cm^{-1} peaks becomes much higher relative to the 1660 and 1071 cm^{-1} peaks (Figure 5) compared to the normal (not ψ-type) VCD spectra of DNA.

The wavenumber of the carbonyl absorption peak continues to shift downward to 1667 cm^{-1} without any signs of slope leveling of as Cr^{3+} concentration increased up to 3 [Cr]/[P] (Figures 4 and 6). This indicates the continuing Cr^{3+} binding to N_7 sites of guanine. The intensity of the carbonyl and symmetric phosphate absorptions remains mostly unchanged between 0.6 and 2 [Cr]/[P] (Figures 6 and 7). At higher Cr^{3+} concentration, the intensity of the carbonyl band starts to increase, while that of the symmetric phosphate band does not change significantly. This behavior might possibly be connected to the saturation of the phosphate binding sites and continuing binding of the metal ions to the base sites even at the highest Cr^{3+} concentration studied. Between 0.6 and 2 [Cr]/[P] the increase of the absorption bands due to Cr^{3+} binding is probably compensated by the absorption intensity decrease due to DNA condensation, hence the overall absorption intensity does not change significantly.

The highest amplitude of the main VCD couplets corresponds to that Cr^{3+} ion concentration (0.6 [Cr]/[P]) at which the peak intensity of the corresponding absorption bands drops sharply (Figures 6 and 7), thus connecting these two phenomena. This reconfirms the conclusion that both spectroscopic changes correspond to the DNA condensation process. Further increase of metal ion concentration reduces the extent of

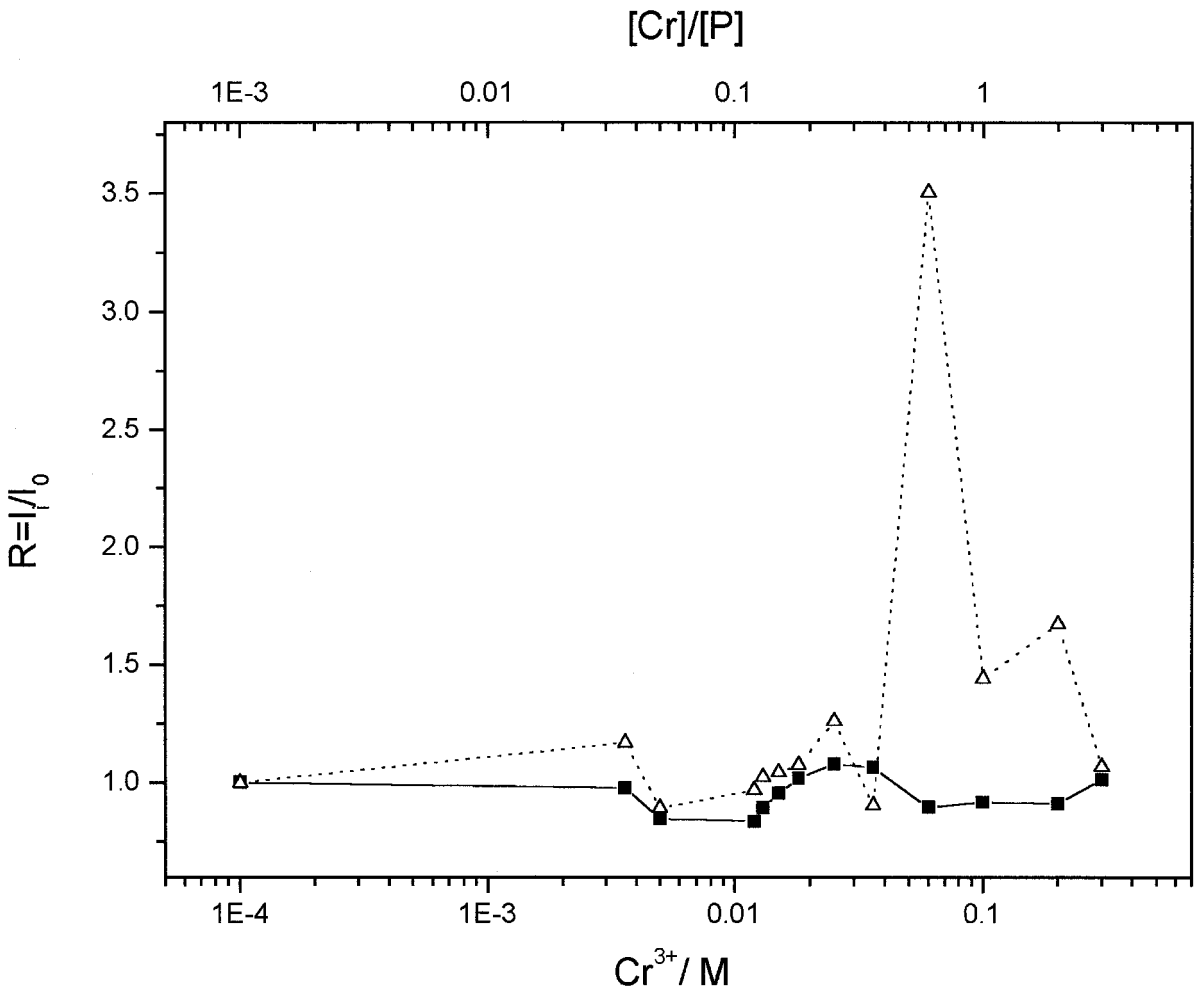

FIGURE 8 Relative absorption and VCD intensity vs Cr^{3+} concentration for the carbonyl absorption at 1682 cm^{-1} plotted on the same scale: (■) intensity of absorption peak; (△) amplitude of VCD couplet.

ψ-type VCD features in both regions up to the point when they mostly disappear (3 [Cr]/[P]). Some variations in the intensity of the VCD couplets can be attributed to a sensitivity of the ψ-type CD intensity to sample preparations.[37] However, the gradual decrease and eventual disappearance of the ψ-type VCD most probably come about because of the increasing size of the condensed particles. As the particle size grows, their dimensions become significantly larger than the wavelengths of light at the absorption bands, and the favorable conditions of strong interaction of the infrared radiation with the condensed particles in the region of interest fades away.[37,42,43] It should be also noted at this point that the condensation process may actually start at much lower Cr^{3+} concentrations than 0.6 [Cr]/[P]. But, it cannot be monitored by ir or VCD due to small particle size or to insufficient particle density. All the changes in the VCD spectrum at 3 [Cr]/[P] compared to the spectrum of DNA without metal ions can therefore be attributed to DNA structural changes that result from extensive Cr^{3+} ion binding at these relatively high metal ion concentrations. The VCD features in both nitrogen base and sugar–phosphate regions together with the continuous shift of the 1682 cm^{-1} carbonyl absorption band confirm the proposed model of Cr^{3+} ion binding to N_7(G) and PO_2^- groups.[10]

Secondary Structure of DNA Molecules Before and After Condensation. IR absorption spectra indicate that DNA secondary structure both before and after the condensation remains within the B-form family (Figures 1–4). This conclusion can be drawn from the presence of the B-form marker bands at 836, 896, and 938 cm^{-1} (Refs. 59, 64, and 80) in absorption for all Cr^{3+} concentrations studied. Neither A-form marker

bands at 810, 865, and 898 cm^{-1} nor Z-form marker band at 800 cm^{-1} (Refs. 10, 59, 64, and 80) can be found in the absorption spectra, signifying that no transition to one of these forms has taken place. Thus, it is confirmed unambiguously that the DNA secondary structure of the ψ-type condensates corresponds to the B-form family, as was reported in other studies.[24,44,45]

Additionally, there was no noticeable DNA denaturation. The carbonyl absorption band at 1682 cm^{-1} shifts down to 1667 cm^{-1} at the highest Cr^{3+} concentration. A similar downward shift of this band is characteristic for DNA denaturation or strand separation.[58,81] A slight peak intensity increase of the 1682 cm^{-1} band can be noted at 3 [Cr]/[P] (Figures 4 and 6). A major intensity increase of this band occurs during DNA denaturation due to increased hyperchromicity.[58,70] These two features may indicate the possibility of DNA denaturation. However, the other features of absorption spectra that are characteristic for DNA denaturation are not present. One of the reliable absorption indicators of DNA denaturation is the shift of the sugar band at 1053 cm^{-1} to 1064 cm^{-1}.[58,59,70,80] Usually, a significant decrease in intensity of the symmetric phosphate absorption band accompanies the shift of 1053 cm^{-1} band during DNA denaturation.[58,64] Neither of these changes occur in the absorption spectra of DNA even at the highest Cr^{3+} concentration (Figures 3, 4, and 7). In general, VCD can provide unambiguous information about DNA denaturation. The helix–coil transition of DNA will result in partial or complete obliteration of VCD signals in both sugar–phosphate and nitrogen base regions.[49,82] Figure 5 clearly shows that the intensity of the VCD couplets of DNA with all Cr^{3+} concentration studied does not become any lower than in the VCD spectrum of DNA alone in both spectroscopic regions. Therefore, both wavenumber shift of the absorption band at 1682 cm^{-1} and its intensity increase at the highest Cr^{3+} concentration are due to metal ion binding to the bases, particularly to N_7(G).

In conclusion, it should be pointed out that the demonstrated ability of VCD spectroscopy to detect DNA condensation and ψ-type changes of VCD spectra characteristic for this process are important for VCD spectroscopic exploration of DNA interactions with various agents, many of which could induce DNA condensation. Although a decrease of ir absorption intensities also signals DNA condensation, these changes are much less pronounced (cf. Figures 4 and 5, see also Figure 8) and can sometimes be obscured by other effects of a condensing agent.

The VCD sensitivity to the condensation process can be also widely used for investigating various aspects of DNA condensation. In fact, a combination of VCD and ir is superior to spectroscopic techniques used to date to study DNA condensation. Along with the ability to determine DNA condensation from VCD spectra, it is possible to obtain *simultaneously* unambiguous information about secondary structure of DNA molecules within the condensed particles from the ir spectra. Both kinds of information are obtained from a single experiment, which means that all the experimental conditions are *exactly* the same and the information about DNA secondary structure indeed corresponds to condensed DNA molecules. In addition, VCD in contrast to ECD makes it possible to study DNA condensation at DNA concentrations much closer to those in living cells.

Numerical Estimation of DNA Charge Neutralization. According to Wilson and Bloomfield,[17] DNA condensation can occur only when at least 89–90% of negative DNA phosphate charges are neutralized by counterions. We estimated numerically the degree of DNA charge neutralization at different concentrations of Cr^{3+} at our experimental conditions. We performed this estimation to verify whether ψ-type VCD spectra, which we attribute to DNA condensation, appear at Cr^{3+} concentration sufficient to neutralize at least 90% of phosphate charges. We used the procedure proposed by Wilson and Bloomfield[17] based on the counterion condensation theory.[16]

The results of the estimation are presented in Figure 9. The large ψ-type VCD spectra, which we attribute to DNA condensation, appear at 0.06*M* Cr^{3+} (Figures 2 and 5). This concentration of Cr^{3+} ions at our experimental conditions corresponds to a phosphate charge neutralization of 92–93%. Therefore, our calculations show that ψ-type VCD spectra appear at Cr^{3+} concentration sufficient to induce DNA condensation. In fact, due to relatively long wavelength of the ir radiation, it is possible to monitor the formation of only relatively large condensed particles comparable to the wavelength of the incident radiation.[37,42,43] However, our AFM experiments show that the DNA condensation process may start at even lower Cr^{3+} concentrations, but the particles formed at these low concentrations are small and not detectable by ir radiation. According to our calculations, the necessary degree of phosphate charge neutralization (90%) is reached at Cr^{3+} concentration higher than 0.007*M* and the condensation may start at any further increase of the Cr^{3+} concentration.

Atomic Force Microscopy

Bloomfield and others[2,4,32,83,84] previously observed toroid and rod formation as a result of DNA conden-

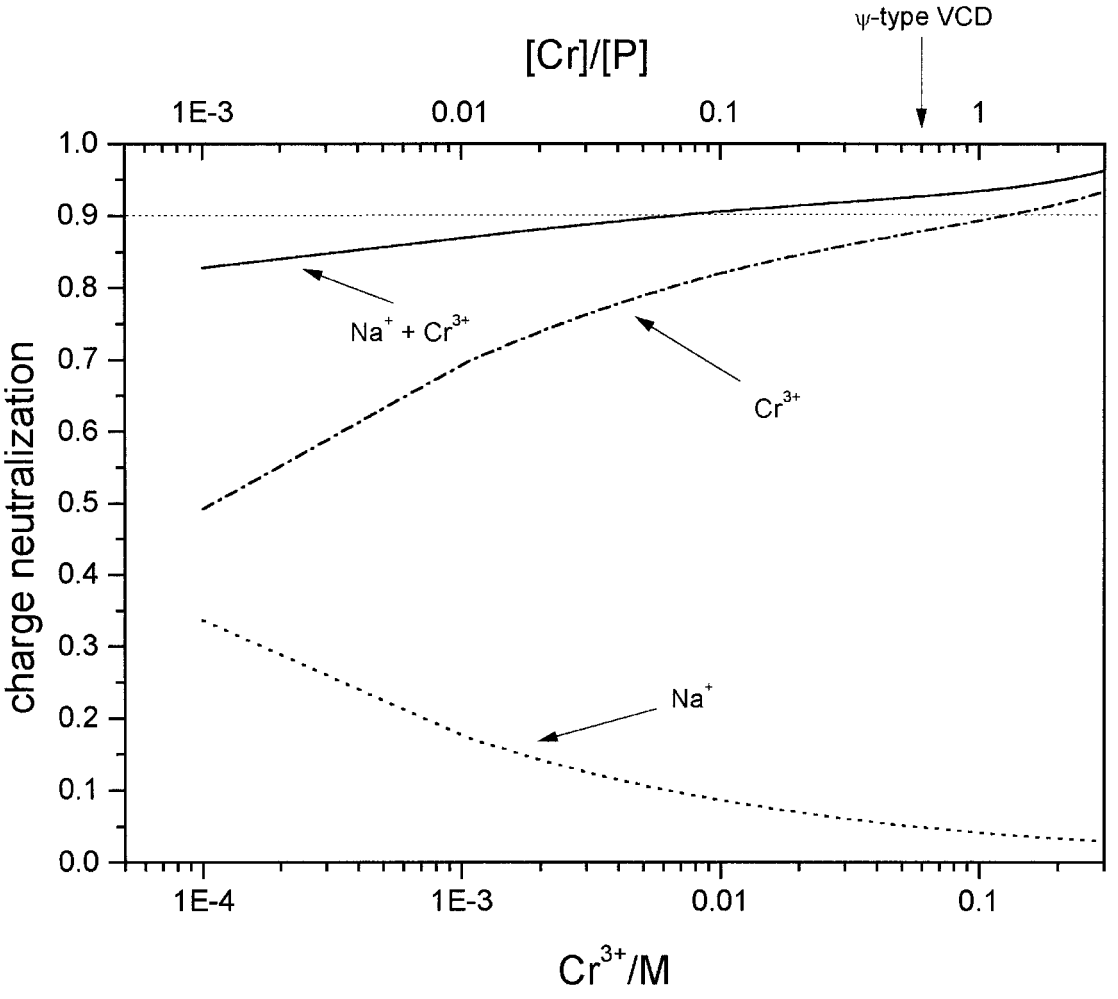

FIGURE 9 Numerical estimation of DNA charge neutralization at different Cr^{3+} concentrations at the conditions used in VCD experiments. Dotted line: DNA charge neutralization by Na^+ ions only; dash-dot line: DNA charge neutralization by Cr^{3+} ions only; solid line: total DNA charge neutralization by Na^+ and Cr^{3+} ions together. Thin horizontal dotted line shows the critical degree of DNA charge neutralization (0.9) necessary for DNA condensation to occur. Arrow at the top axes indicates the Cr^{3+} concentration at which the ψ-type VCD spectra appear (0.06*M* Cr^{3+} or 0.6 [Cr]/[P]).

sation induced by Co^{3+} hexamine, spermidine, etc. The authors imaged dry samples by using electron microscopy. In our study the samples were always fully hydrated, so DNA was imaged under near-physiological conditions, which helped to avoid any complex disturbance during drying. Structures and conformations of DNA complexes can be sensitive to drying artifacts.[12] DNA with length 850 and 3000 base pairs was used. Using different conditions we were able to attach both DNA to mica without addition of Cr^{3+} ions and with several concentrations of Cr^{3+} ions added (Figures 10–13). The DNA concentration used in AFM experiments (80 μg/mL) was significantly lower than that used in VCD measurements in order to be able to observe visually the process of condensation.

We observed the increase of DNA folding due to binding of Cr^{3+} ions to DNA strands. With the increase of Cr^{3+} concentration we could monitor gathering of DNA molecules (Figure 11). At 1 m*M* Cr^{3+} concentration ([Cr]/[P] = 3.8) we observed formation of loose flower-like structures, similar to that observed previously in the presence of spermine (Figure 11).[12] Small condensed parts at the ends of DNA strands or at the DNA segments crossing sites can be seen as well as separated DNA strands. This indicates that DNA condensation can start as folding of one separate strand as well as cooperative interactions

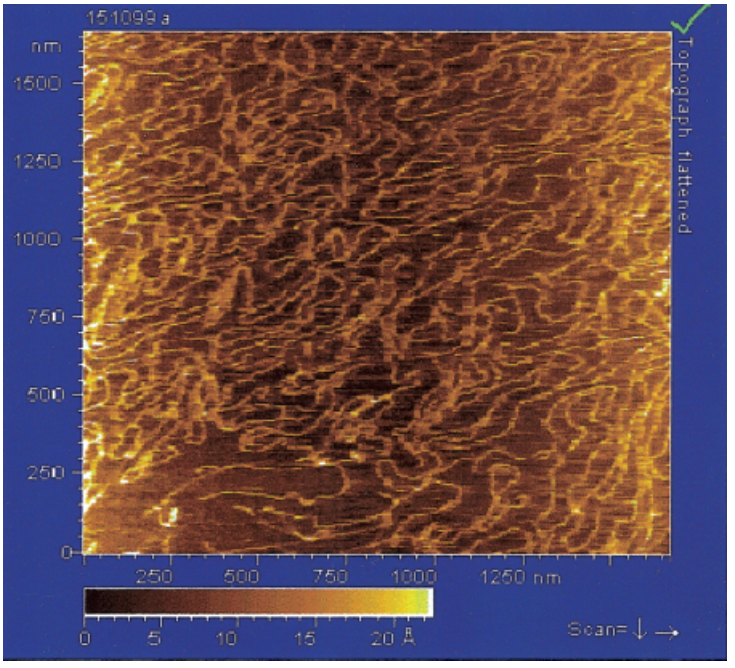

FIGURE 10 AFM image of DNA. DNA length is 3000 bp.

between DNA segments. The further increase of Cr^{3+} concentration (2 m*M*) leads to the formation of the complexes, which are globular and smaller in size (Figure 12). These complexes form larger particles due to the aggregation of previously formed particles. Both smaller and larger aggregates were observed. After a certain Cr^{3+} concentration (5 m*M*), it was impossible to resolve the individual DNA strands inside of these formations (Figure 13). The formations had various shapes, tending, however, to be spherical on average. At yet higher metal ion concentration, we were unable to attach the aggregates to mica, possibly

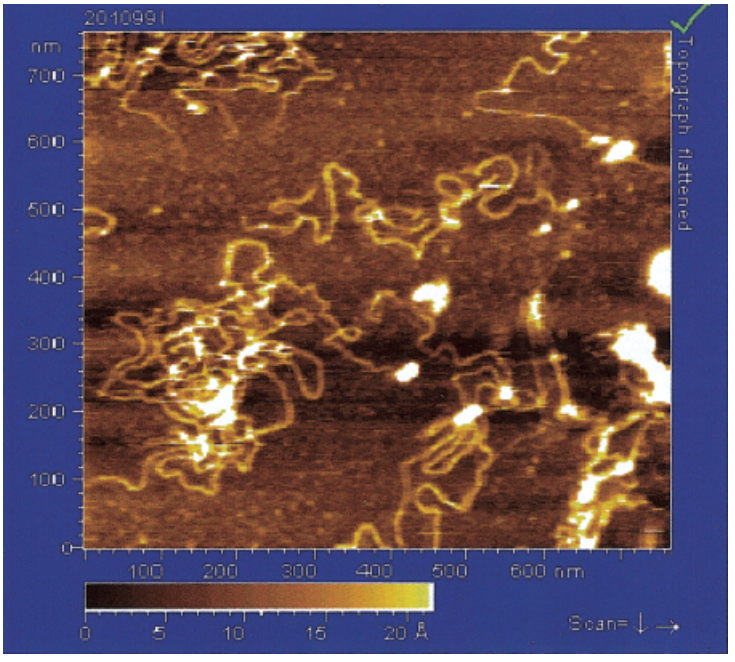

FIGURE 11 AFM image of DNA with 1 m*M* of Cr^{3+} ions. DNA length is 3000 bp.

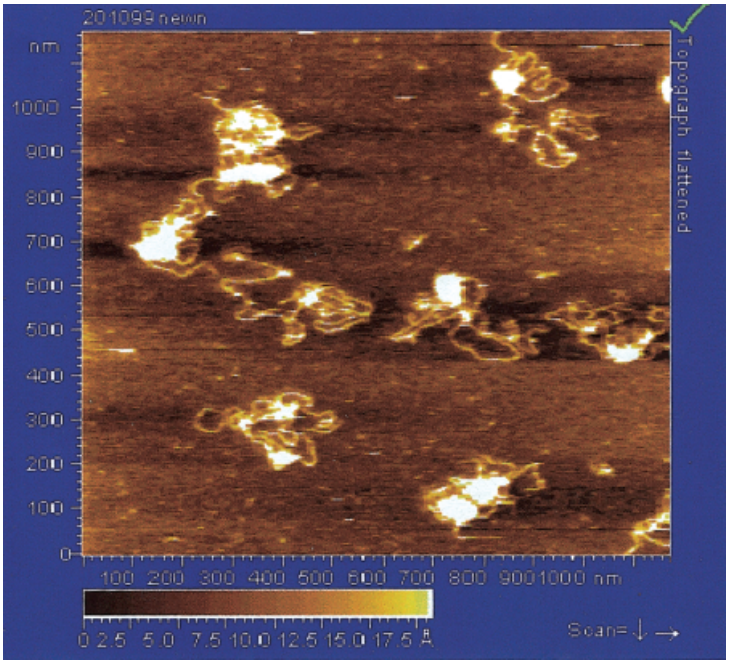

FIGURE 12 AFM image of DNA with 2 m*M* of Cr^{3+} ions. DNA length is 3000 bp.

due to their large size and very high density. The formation of large dense aggregates indicates that a great extent of electrical charge neutralization occurred, which is the major driving force of DNA condensation. Both DNA types show similar results, although for 3000 base pairs tight DNA condensates were formed at higher Cr^{3+} ion concentration. When DNA or DNA complexes with Cr^{3+} ions were adsorbed to the mica surface, no further complex tightening was observed during 30–60 min of imaging. Modified (PLL) mica surface itself did not cause any linear DNA condensation or folding (Figure 10).

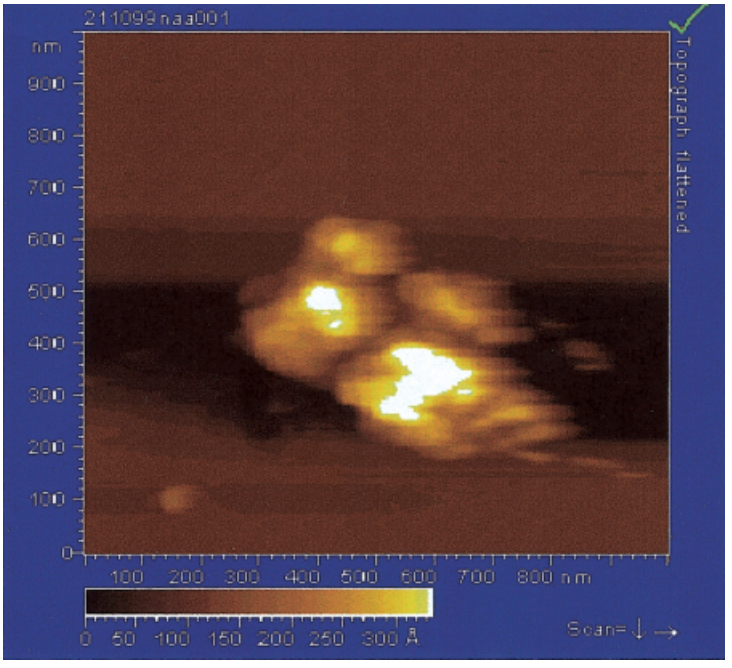

FIGURE 13 AFM image of DNA with 5 m*M* of Cr^{3+} ions. DNA length is 3000 bp.

We did not observe formation of small tight rods or toroids because multimolecular interactions prevailed due to relatively high DNA concentrations, which suppressed intramolecular condensation. Intramolecular condensation in sufficiently dilute DNA solutions [$10^{-6}M$ (P)] is known to be favorable for toroid and rod formation.[3,4]

CONCLUSIONS

Interaction of natural calf thymus DNA with Cr^{3+} ions was studied at room temperature by means of VCD and ir spectroscopy and AFM microscopy. Cr^{3+} ion binding mainly to N_7(G) and to phosphate groups was demonstrated. An anomalous fourfold increase of VCD intensity with just minor changes in absorption spectra was observed for [Cr]/[P] between 0.6 and 1. This increase of VCD intensity was similar to the intensity increase occurring in ECD spectra during ψ-type DNA condensation. In addition to enormously increased intensity, the VCD spectra showed other features typical for ECD ψ-spectra, e.g., long "tails" in nonabsorbing regions. Following the theory,[37,42,43] the anomalous VCD spectra were assigned to DNA condensation with formation of large and dense particles of a size comparable to the wavelength of the probing ir beam. In order to produce the ψ-type VCD and ECD spectra, particles must consist of regularly arranged double-helical DNA molecules, providing large-scale helicity. No DNA denaturation was observed even at the highest concentration of Cr^{3+} ions studied, namely 0.3M Cr^{3+} (3 [Cr]/[P]). DNA secondary structure remained within the B-form family before and after the condensation as revealed by ir absorption. The combination of VCD and ir absorption spectroscopy proved to be an unique method for investigating DNA condensation. Along with the ability to determine the onset of DNA condensation, this combination can provide information about the secondary structure of DNA molecules within condensed particles in the same experiment, i.e., at exactly the same experimental conditions.

The results of the numerical estimation of the degree of DNA phosphate charge neutralization at different Cr^{3+} concentrations in our experimental conditions confirmed that ψ-type VCD spectra appeared at the Cr^{3+} concentrations high enough to neutralize the necessary amount of DNA charge for the DNA condensation to take place.

AFM study confirmed DNA condensation by Cr^{3+} ions in tight DNA formations, which is one of the conditions necessary for observing ψ-type VCD spectra. The increase in Cr^{3+} ion concentration changes the structure of condensates from loose flower-like ones to highly packed dense spheres. The results from VCD and ir absorption together with AFM were found to be complimentary and in good qualitative agreement.

We would like to thank Prof. D. Lando for kindly provided calf thymus DNA for VCD and AFM measurements. We also would like to thank Dr. S. P. Lees-Miller for the samples of *E. coli* DNA for AFM measurements. We express our gratitude to the Department of Chemistry at the University of Calgary for providing the necessary infrastructure for the research to take place. Funding is gratefully acknowledged from the Natural Sciences and Research Council of Canada to H. Wieser and D. Cramb, as well as from IIPP and Travis Chemicals to D. Cramb.

REFERENCES

1. Ono, M. Y.; Spain, E. M. J Am Chem Soc 1999, 121, 7330–7334.
2. Arscott, P. G.; Li, A. Z.; Bloomfield, V. A. Biopolymers 1990, 30, 619–630.
3. Bloomfield, V. A. Biopolymers 1998, 44, 269–282.
4. Widom, J.; Baldwin, R. L. J Mol Biol 1980, 144, 431–453.
5. Bloomfield, V. A. Biopolymers 1991, 31, 1471–1481.
6. Lin, Z.; Wang, C.; Feng, X.; Liu, M.; Li, J.; Bai, C. Nucleic Acid Res 1998, 26, 3228–3234.
7. Osterberg, R.; Persson, D.; Bjursell, G. J Biomol Struct Dyn 1984, 2, 285–290.
8. Gersanovski, D.; Colson, P.; Houssier, C.; Fredericq, E. Biochim Biophys Acta 1985, 824, 313–323.
9. Tajmir-Riahi, H. A.; Ahmad, R.; Naoui, M. J Biomol Struct Dyn 1993, 10, 865–877.
10. Arakawa, H.; Ahmad, R.; Naoui, M.; Tajmir-Riahi, H. A. J Biol Chem 2000, 275, 10150–10153.
11. Allen, M. J.; Bradbury, E. M.; Balhorn, R. Nucleic Acid Res 1997, 25, 2221–2226.
12. Hansma, H. G.; Golan, R.; Hsieh, W.; Lollo, C. P.; Mullen-Ley P.; Kwoh, D. Nucleic Acid Res 1998, 26, 2481–2487.
13. Lerman, L. S. Proc Natl Acad Sci USA 1971, 68, 1886–1890.
14. Fang, Y.; Hoh, J. H. Nucleic Acid Res 1998, 26, 588–593.
15. Leonenko, Z. V.; Merkle, D.; Lees-Miller, S. P.; Cramb, D. T. Langmuir 2002, in press.
16. Manning, G. S. Quart Rev Biophys 1978, 11, 179–246.
17. Wilson, R.W.; Bloomfield, V. A. Biochemistry 1979, 18, 2192–2196.
18. Yurgaitis, A. P.; Lazurkin, Y. S. Biopolymers 1981, 20, 967–975.
19. Widom, J.; Baldwin, R. L. Biopolymers 1983, 22, 1595–1620.
20. Schellman, J. A.; Parthasarathy, N. J Mol Biol 1984, 175, 313–329.

21. Knoll, D. A.; Fried, M. G.; Bloomfield, V. A. In Structure & Expression. Volume 2—DNA and Its Drug Complexes; Sarma, R. H., Sarma, M. H., Eds.; Adenine Press: Schenectady, NY, 1988; pp 123–145.
22. Jordan, C. F.; Lerman, L. S.; Venable, J. H. Nature New Biol 1972, 236, 67–70.
23. Cheng, S. M.; Mohr, S. C. FEBS Lett 1974, 49, 37–42.
24. Cheng, S. M.; Mohr, S. C. Biopolymers 1975, 14, 663–674.
25. Shin, Y. A.; Eichhorn, G. L. Biopolymers 1984, 23, 325–335.
26. Maestre, M. F.; Reich, C. Biochemistry 1980, 19, 5214–5223.
27. Evdokimov, Y. M.; Platonov, A. L.; Tikhonenko, A. S.; Varshavsky, Y. M. FEBS Lett 1972, 23, 180–184.
28. Bloomfield, V. A.; He, S.; Li, A.; Arscott, P. B. Biochem Soc Trans 1991, 19, 496–496.
29. He, S.; Arscott, P. G.; Bloomfield, V. A. Biopolymers 2000, 53, 329–341.
30. Takahashi, M.; Yoshikawa, K.; Vasilevskaya, V. V.; Khokhlov, A. R. J Phys Chem B 1997, 101, 9396–9401.
31. Ma, C.; Bloomfield, V. A. Biophys J 1994, 67, 1678–1681.
32. Chattoraj, D. K.; Gosule, L. C.; Schellman, J. A. J Mol Biol 1978, 121, 327–337.
33. Golan, R.; Pietrasanta, L. I.; Hsieh, W.; Hansma, H. G. Biochemistry 1999, 38, 14069–14076.
34. Hansma, H. G. Ann Rev Phys Chem 2001, 52, 71–92.
35. Liu, D.; Wang, C.; Li, J.; Tan, Z.; Bai, C. J Biomol Struct Dyn 2000, 18, 1–9.
36. Potaman, V. N.; Shlyakhtenko, L. S. Mol Biol 1982, 16, 730–736.
37. Keller, D.; Bustamante, C. J Chem Phys 1986, 84, 2972–2980.
38. Allison, S. A.; Herr, J. C.; Schurr, J. M. Biopolymers 1981, 20, 469–488.
39. Lerman, L. S. Cold Spring Harbor Symp Quant Biol 1973, 38, 59–73.
40. Brunner, W. C.; Maestre, M. F. Biopolymers 1974, 13, 345–357.
41. Weinberger, S.; Berman, C.; Minsky, A. J Am Chem Soc 1988, 110, 8231–8232.
42. Keller, D.; Bustamante, C. J Chem Phys 1986, 84, 2961–2971.
43. Kim, M. H.; Ulibarri, L.; Keller, D.; Maestre, M. F.; Bustamante, C. J Chem Phys 1986, 84, 2981–2989.
44. Maniatis, T.; Venable, J. H.; Lerman, L. S. J Mol Biol 1974, 84, 37–64.
45. Zacharias, W.; Martin, J. C.; Wells, R. D. Biochemistry 1983, 22, 2398–2405.
46. Annamalai, A.; Keiderling, T. A. J Am Chem Soc 1987, 109, 3125–3132.
47. Gulotta, M.; Goss, D. J.; Diem, M. Biopolymers 1989, 28, 2047–2058.
48. Diem, M. SPIE Proc 1991, 1432, 28–36.
49. Yang, L.; Keiderling, T. A. Biopolymers 1993, 33, 315–327.
50. Wang, L.; Keiderling, T. A. Nucleic Acid Res 1993, 21, 4127–4132.
51. Wang, L.; Pancoska, P.; Keiderling, T. A. Biochemistry 1994, 33, 8428–8435.
52. Keiderling, T. A. In Circular Dichroism and the Conformational Analysis of Biomolecules; Fasman, G. D., Ed.; Plenum Press: New York, 1996; pp 555–597.
53. Birke, S.; Diem, M. Biophys J 1995, 68, 1045–1049.
54. Andrushchenko, V. V.; van de Sande, J. H.; Wieser, H. Vibr Spectrosc 1999, 19, 341–345.
55. Andrushchenko, V. V.; van de Sande, J. H.; Wieser, H.; Kornilova, S. V.; Blagoi, Y. P. J Biomol Struct Dyn 1999, 17, 545–560.
56. Andrushchenko, V. V.; McCann, J. L.; van de Sande, J. H.; Wieser, H. Vibr Spectrosc 2000, 22, 101–109.
57. Tsuboi, M. Appl Spectrosc Rev 1969, 3, 45–90.
58. Tsuboi, M. In Basic Principles in Nucleic Acid Chemistry; Ts'o, P. O. P., Ed.; Academic Press: New York, 1974; pp 400–451.
59. Taillandier, E.; Liquier, J.; Taboury, J. A. In Advances in Infrared and Raman Spectroscopy; Clark, R. J. H., Hester, R. E., Eds.; Wiley Heyden: New York, 1985; Vol 12, pp 65–114.
60. Lando, D. Y.; Egorova, V. P.; Krot, V. I.; Akhrem, A. A. Mol Biol 1996, 30, 418–421.
61. Tsankov, D.; Eggimann, T.; Wieser, H. Appl Spectrosc Rev 1995, 49, 132–138.
62. Han, W.; Lindsay, S. M.; Jing, T. Appl Phys Lett 1996, 69, 1–3.
63. Han, W.; Lindsay, S. M. Appl Phys Lett 1998, 72, 1656–1658.
64. Taillandier, E. Structure and Methods, Volume 3: DNA & RNA; Sarma, R. H., Sarma, M. H., Eds.; Adenine Press: Schenectady, NY, 1990; pp 073–078.
65. Wang, L.; Keiderling, T. A. Biochemistry 1992, 31, 10265–10271.
66. Wang, L.; Yang, L.; Keiderling, T. A. Biophys J 1994, 67, 2460–2467.
67. Zhong, W.; Gulotta, M.; Goss, D. J.; Diem, M. Biochemistry 1990, 29, 7485–7491.
68. Maharaj, V. Ph.D. thesis, University of Calgary, 1996.
69. Bose, P. K.; Polavarapu, P. L. J Am Chem Soc 1999, 121, 6094–6095.
70. Tajmir-Riahi, H. A.; Naoui, M.; Ahmad, R. Biopolymers 1993, 33, 1819–1827.
71. Keller, P. B.; Hartman, K. A. Nucleic Acids Res 1986, 14, 8167–8182.
72. Alex, S.; Dupuis, P. Inorg Chim Acta 1988, 157, 271–281.
73. Sponer, J.; Burda, J.; Sabat, M.; Leszczynski, J.; Hobza, P. J Phys Chem A 1998, 102, 5951–5957.
74. Fritzsche, H.; Zimmer, C. Eur J Biochem 1968, 5, 42–44.
75. Zimmer, C.; Luck, G.; Fritzsche, H.; Triebel, H. Biopolymers 1971, 10, 441–463.
76. Tsapakos, M. J.; Wetterhahn, K. E. Chem-Biol Interact 1983, 46, 265–277.

77. Wolf, T.; Kasemann, R.; Ottenwalder, H. Carcinogenesis 1989, 10, 655–659.
78. Tajmir-Riahi, H. A.; Langlais, M.; Savoie, R. Nucleic Acid Res 1988, 16, 751–762.
79. Kornilova, S. V.; Hackl, E. V.; Kapinos, L. E.; Andrushchenko, V. V.; Blagoi, Y. P. Acta Biochim Pol 1998, 45, 107–117.
80. Taillandier, E.; Liquier, J. In Methods in Enzymology; Lilley, D., Dahlberg, J., Eds.; Academic Press: New York, 1992; Vol 211, pp 307–335.
81. Parker, F. S. Applications of Infrared Spectroscopy in Biochemistry, Biology and Medicine; Plenum Press: New York, 1971.
82. Andrushchenko, V. V.; van de Sande, J. H.; Blagoi, Yu. P.; Wieser, H. J Biomol Struct Dyn 2002, 19, 889–906.
83. Marx, K. A.; Ruben, G. C. Nucleic Acid Res 1983, 11, 1839–1854.
84. Plum, G. E.; Arscott, P. G.; Bloomfield, V. A. Biopolymers 1990, 30, 631–643.